Liquid Crystals
Publication details, including instructions for authors and subscription information:
http://www.informaworld.com/smpp/title~content=t713926090

Stable configurations in hybrid nematic cells in relation to thickness and surface order

H. G. Galabova; N. Kothekar; D. W. Allender

Online publication date: 29 June 2010

LIQUID CRYSTALS, 1997, VOL. 23, NO. 6, 803–811

Stable configurations in hybrid nematic cells in relation to thickness and surface order

by H. G. GALABOVA*, N. KOTHEKAR and D. W. ALLENDER
Liquid Crystal Institute and Physics Department, Kent State University, Kent, Ohio 44242, USA

(*Received 4 June 1997; accepted 7 July 1997*)

The phase diagram of equilibrium configurations in thin hybrid nematic cells has been investigated in the framework of Landau–de Gennes theory extended to include weak surface anchoring. Surface interactions linear in the tensor order parameter were assumed and biaxiality was induced by the surfaces. It was found that in addition to the usual configuration where the director bends continuously from one plate to the other, there is also a possible configuration where bend does not occur, but where there is an eigenvalue exchange; i.e. the eigenvector of the tensor order parameter associated with the eigenvalue of the largest magnitude is different in different regions of the cell. Furthermore, for very small cell thickness a third possibility occurs: the eigenvector corresponding to the eigenvalue with the largest magnitude is uniform throughout the cell; it is either parallel or perpendicular to both plates depending upon the dominant surface interaction. Continuous transitions occur between the different configurations.

1. Introduction

The elastic properties of nematic liquid crystals are usually studied using Frank theory [1] where the nematic phase is described in terms of a director $\hat{\mathbf{n}}$ along which the molecules are preferentially oriented, and a set of elastic constants which depend on the degree of orientational order S. The nematic director is considered to vary in space, but the degree of order is assumed to be spatially independent and affected only by temperature.

It is of interest to know how the introduction of spatial dependence in the degree of order would affect the description of phenomena usually interpreted in terms of Frank elastic theory. Generalization of Frank theory to include variable degree of order was done by Ericksen [2] and implemented in a simplified version by other authors [3–5] who arrived at the conclusion that the generalized theory may be suitable for describing line and plane defects. However, both Frank theory and its generalization are applicable only to uniaxial nematic phases. As is well known, liquid crystal molecules that form nematic phases are not axially symmetric. However, bulk nematic phases in low molecular weight thermotropic systems are so far observed to be uniaxial. Because surfaces are anticipated to induce biaxiality, the description of nematic phases in restricted geometries should allow for that possibility.

*Author for correspondence.

In the framework of the Landau–de Gennes formalism [6], the properties of nematic liquid crystals are described in terms of a tensor order parameter which in the case of a biaxial nematic has five independent components, all spatially dependent. It was suggested by Gartland *et al.* [7] that the boundary conditions imposed on the liquid crystal can be satisfied by a biaxial configuration where an eigenvalue exchange occurs; i.e. the eigenvector of the tensor order parameter associated with the eigenvalue of the largest magnitude switches from one of the local principal axes to another. In a theoretical study of a hybrid nematic cell having homeotropic alignment at one plate and homogeneous at the other [8], a second order transition was found to occur, from the usual configuration where the director bends continuously between the bounding plates, to an eigenvalue exchange configuration when the cell thickness is decreased. However, only strong anchoring and uniaxial order at the surfaces were considered. It is relevant also to take into account the finite anchoring energy between the liquid crystal and walls, as well as the biaxial order at the homogeneous surface. In related work reported elsewhere [9] the effect of a weak surface interaction was included for a twisted nematic film where an eigenvalue exchange configuration was also found.

Weak anchoring conditions in the framework of Landau–de Gennes theory have been a subject of theoretical investigation ever since the work of Sheng on weak homeotropic anchoring in a semi-infinite sample

0267–8292/97 $12·00

[10]. Throughout the years the cases of both semi-infinite and finite nematic samples with homeotropic [10–12] and planar [13–16] surface anchoring have been studied. In this work we turn our attention to the theoretical treatment of homogeneous surface anchoring in the framework of Landau–de Gennes theory, and we further investigate the different configurations that can be realized in a hybrid nematic cell, this time allowing for weak surface interactions and biaxiality at the homogeneous plate. We also study the effect of variable anchoring on the conditions required for a bend to eigenvalue exchange transition to occur.

2. Theory

We consider a nematic liquid crystal confined between two bounding plates placed at $\xi=0$ and $\xi=d$ in the lab reference frame having orthogonal unit vectors ξ, $\hat{\nu}$, and ζ (figure 1). The plate at $\xi=0$ favours homeotropic alignment with the easy direction described by the unit vector ξ, and the plate at $\xi=d$ favours homogeneous alignment with an in-plane easy axis along the unit vector $\hat{\nu}$. At any point between the plates, the nematic can be described by a biaxial tensor order parameter diagonal in the reference frame of the local principal axes $\hat{\mathbf{n}}$, $\hat{\mathbf{m}}$, and $\hat{\mathbf{l}}$. We assume that $\hat{\mathbf{l}}$ is along $\zeta=\xi\times\hat{\nu}$ throughout the cell, $\hat{\mathbf{n}}=\cos\theta\xi+\sin\theta\hat{\nu}$, and $\hat{\mathbf{m}}=-\sin\theta\xi+\cos\theta\hat{\nu}$, where θ is the bend angle. At any ξ the nematic order is assumed to be uniform in the ν–ζ plane. Thus, the spatial dependence of the tensor order parameter is reduced to only one spatial coordinate, i.e. the ξ coordinate. These assumptions, together with the equal elastic constants approximation used in our calculations, rule out the possibility of striped configurations [17–20] which will not be considered here.

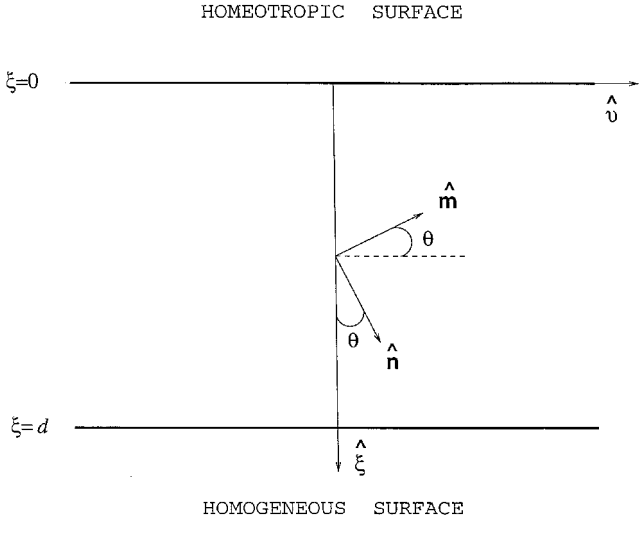

Figure 1. Hybrid cell geometry: homeotropic alignment at $\xi=0$ and homogeneous at $\xi=d$; $\hat{\mathbf{l}}=\zeta=\xi\times\hat{\nu}$ throughout the cell.

At any ξ, the tensor order parameter in the lab reference frame is given by

$$Q_{ij}=\frac{S}{2}(3n_in_j-\delta_{ij})+\frac{P}{2}(m_im_j-l_il_j) \tag{1}$$

where S is the usual uniaxial order parameter and P is a measure of the biaxiality.

In terms of S, P and the bend angle θ, the tensor order parameter has the following form:

$$Q=\frac{1}{4}\begin{pmatrix} S+P+(3S-P)\cos 2\theta & (3S-P)\sin 2\theta & 0 \\ (3S-P)\sin 2\theta & S+P-(3S-P)\cos 2\theta & 0 \\ 0 & 0 & -2(S+P) \end{pmatrix}. \tag{2}$$

Here all three parameters S, P, and θ are spatially dependent.

The tensor above has a more convenient representation [7, 8] given by

$$Q=\frac{1}{6^{1/2}}\begin{pmatrix} z+3^{1/2}x & 3^{1/2}y & 0 \\ 3^{1/2}y & z-3^{1/2}x & 0 \\ 0 & 0 & -2z \end{pmatrix}, \tag{3}$$

where

$$x=\frac{2^{1/2}}{4}(3S-P)\cos 2\theta$$

$$y=\frac{2^{1/2}}{4}(3S-P)\sin 2\theta$$

$$z=\frac{6^{1/2}}{4}(S+P).$$

The Landau–de Gennes free energy of the system, allowing for weak surface interactions, can be written in the form

$$F=\int f_b\,\mathrm{d}V+\int(f_{s0}+f_{s1})\,\mathrm{d}S, \tag{4}$$

where

$$f_b=\frac{1}{2}A\,trQ^2-\frac{1}{3}B\,trQ^3+\frac{1}{4}C(trQ^2)^2$$

$$+\frac{1}{2}L_1(\partial_iQ_{jk})(\partial_iQ_{jk})+\frac{1}{2}L_2(\partial_iQ_{ij})(\partial_kQ_{kj}) \tag{5}$$

is the bulk free energy density including elastic terms [21]. The elasticity here is connected not only with variations in the molecular orientation, but also with

variations in the degrees of order S and P. The term

$$f_{s0} = G_0 Q_{ij} \xi_i \xi_j \tag{6}$$

is the surface free energy contribution from the homeotropic surface. It corresponds to having uniaxial order at the surface and when $G_0 < 0$, this term favours alignment perpendicular to the homeotropic plate. The surface free energy contribution from the homogeneous surface has the form

$$f_{s1} = G_1 Q_{ij} \xi_i \xi_j + B_1 Q_{ij} \hat{\nu}_i \hat{\nu}_j. \tag{7}$$

The term with B_1, where $B_1 < 0$, favours alignment along the easy axis $\hat{\nu}$, and the term with G_1, G_1 being positive, favours orientation in the plane of the surface and introduces biaxiality at the homogeneous plate. If the surface is to favour alignment along the easy axis $\hat{\nu}$, at any given B_1 not all values are allowed for the G_1 coefficient. Calculations with a semi-infinite cell have shown that the allowed values of G_1 are those for which $0 \leqslant G_1 \leqslant |B_1|$, where $G_1 = 0$ corresponds to uniaxial order at the surface.

Scaled to dimensionless units, the Landau–de Gennes free energy has the form

$$\begin{aligned} \mathscr{F} = \int_0^1 \Bigg\{ & \frac{a}{2}(x^2+y^2+z^2) - bz\left(x^2+y^2-\frac{z^2}{3}\right) \\ & + \frac{1}{4}(x^2+y^2+z^2)^2 + \frac{l_1}{2}[(x')^2+(y')^2+(z')^2] \\ & + \frac{l_2}{2}\left[\left(\frac{1}{6^{1/2}}z' + \frac{1}{2^{1/2}}x'\right)^2 + \frac{1}{2}(y')^2\right]\Bigg\} \mathrm{d}\eta \\ & + \omega_{x1}x(1) - \omega_{z1}z(1) - \frac{\omega_0}{6^{1/2}}z(0) - \frac{\omega_0}{2^{1/2}}x(0), \end{aligned} \tag{8}$$

where $\mathscr{F} = F/\mathscr{A} Cd$, $a = A/C$, $b = B/(6^{1/2}C)$, $l_{1,2} = L_{1,2}/Cd^2$, $\omega_{z1} = -(G_1+B_1)/(6^{1/2}Cd)$, $\omega_{x1} = (G_1-B_1)/(2^{1/2}Cd)$, and $\omega_0 = G_0/Cd$. The area of the cell is denoted by $\mathscr{A}$, and $\eta = \xi/d$. The coupling coefficients ω_0, ω_{x1}, and ω_{z1} are all positive and the signs of the terms with which they enter the free energy are chosen in such a way that alignment along ξ is favoured at the homeotropic surface, and alignment along $\hat{\nu}$ at the homogeneous one.

3. Minimization of the free energy

To minimize the free energy $\mathscr{F}$ we follow the standard variational procedure [22]; that is, we introduce new functions $f_x(\eta)$, $f_y(\eta)$, and $f_z(\eta)$, and a scale factor α such that the varied paths are given by

$$\begin{aligned} x(\eta, \alpha) &= x(\eta) + \alpha f_x(\eta) \\ y(\eta, \alpha) &= y(\eta) + \alpha f_y(\eta) \\ z(\eta, \alpha) &= z(\eta) + \alpha f_z(\eta). \end{aligned}$$

For strong anchoring at both plates $f_{x,y,z}(\eta = 0) = f_{x,y,z}(\eta = 1) = 0$ and $x(\eta)$, $y(\eta)$, and $z(\eta)$ satisfy the Euler–Lagrange equations obtained by minimizing the bulk free energy only. However, in the case of weak surface anchoring, the values of the functions at the end points are not fixed. This fact does not change the Euler–Lagrange equations, but affects only the boundary conditions for the problem. Assuming that $f_x(\eta)$, $f_y(\eta)$, and $f_z(\eta)$ are independent of each other and that $f_{x,y,z}(\eta = 0)$ can be varied independently of $f_{x,y,z}(\eta = 1)$, we find the following differential equations for $x(\eta)$, $y(\eta)$, and $z(\eta)$:

$$\begin{aligned} & \left(1 + \frac{l_2}{2l_1}\right)\frac{\mathrm{d}^2x}{\mathrm{d}\eta^2} + \frac{l_2}{12^{1/2}l_1}\frac{\mathrm{d}^2z}{\mathrm{d}\eta^2} - \frac{a}{l_1}x \\ & \quad + 2\frac{b}{l_1}zx - \frac{1}{l_1}x(x^2+y^2+z^2) = 0 \\ & \left(1 + \frac{l_2}{2l_1}\right)\frac{\mathrm{d}^2y}{\mathrm{d}\eta^2} - \frac{a}{l_1}y \\ & \quad + 2\frac{b}{l_1}yz - \frac{1}{l_1}y(x^2+y^2+z^2) = 0 \\ & \left(1 + \frac{l_2}{6l_1}\right)\frac{\mathrm{d}^2z}{\mathrm{d}\eta^2} + \frac{l_2}{12^{1/2}l_1}\frac{\mathrm{d}^2x}{\mathrm{d}\eta^2} - \frac{a}{l_1}z \\ & + \frac{b}{l_1}(x^2+y^2-z^2) - \frac{1}{l_1}z(x^2+y^2+z^2) = 0, \end{aligned} \tag{9}$$

with boundary conditions given by

$$\begin{aligned} \left(1 + \frac{l_2}{2l_1}\right)x'(1) + \frac{l_2}{12^{1/2}l_1}z'(1) + \frac{\omega_{x1}}{l_1} &= 0 \\ \left(1 + \frac{l_2}{2l_1}\right)x'(0) + \frac{l_2}{12^{1/2}l_1}z'(0) + \frac{\omega_0}{2^{1/2}l_1} &= 0 \\ \left(1 + \frac{l_2}{2l_1}\right)y'(1) &= 0 \\ \left(1 + \frac{l_2}{2l_1}\right)y'(0) &= 0 \\ \left(1 + \frac{l_2}{6l_1}\right)z'(1) + \frac{l_2}{12^{1/2}l_1}x'(1) - \frac{\omega_{z1}}{l_1} &= 0 \\ \left(1 + \frac{l_2}{6l_1}\right)z'(0) + \frac{l_2}{12^{1/2}l_1}x'(0) + \frac{\omega_0}{6^{1/2}l_1} &= 0. \end{aligned} \tag{10}$$

For calculational simplicity the equal elastic constants approximation ($l_2 = 0$) was used. With this approximation the equations and the boundary conditions are simplified to

$$\frac{d^2x}{d\eta^2} - \frac{a}{l_1}x + 2\frac{b}{l_1}zx - \frac{1}{l_1}x(x^2+y^2+z^2) = 0$$

$$\frac{d^2z}{d\eta^2} - \frac{a}{l_1}z + \frac{b}{l_1}(x^2+y^2-z^2) - \frac{1}{l_1}z(x^2+y^2+z^2) = 0,$$

$$\frac{d^2y}{d\eta^2} - \frac{a}{l_1}y + 2\frac{b}{l_1}yz - \frac{1}{l_1}y(x^2+y^2+z^2) = 0 \tag{11}$$

and

$$x'(1) = -\frac{\omega_{x1}}{l_1}$$

$$x'(0) = -\frac{\omega_0}{2^{1/2}l_1}$$

$$y'(1) = 0$$

$$y'(0) = 0 \tag{12}$$

$$z'(1) = \frac{\omega_{z1}}{l_1}$$

$$z'(0) = -\frac{\omega_0}{6^{1/2}l_1}$$

respectively. The equations were solved numerically using the code COLNEW [23] which solves mixed systems of ordinary differential equations.

4. Results and discussion

Using the method of analysis developed in ref. [8] we consider the value of $y = \frac{1}{4}(3S - P)\sin 2\theta$ as a parameter to distinguish between the configuration where the director $\hat{\mathbf{n}}$ bends between the two plates and the predominantly biaxial configurations where eigenvalue exchanges occur. For strong anchoring, $y = 0$ at each surface because θ is either 0 or $\pi/2$. Furthermore, $y(\eta)$ is symmetric with respect to the middle of the cell. Therefore, its maximum value is $y_{max} = y(0{\cdot}5)$ and if $y(0{\cdot}5) \neq 0$, bend has occurred. Conversely, if bend does not occur, $y(0{\cdot}5) = 0$. However, when the anchoring is weak, y does not have to vanish at the plates and does not have to take its maximum value in the middle of the cell. Even in this case though, $y_{max} = 0$ indicates that no bend has occurred. By examining the behaviour of the bend angle θ, it was found that whenever $y_{max} \neq 0$, bend does happen. To illustrate when bend occurs, in figure 2 we show the maximum value of y as a function of $D^2 = 1/l_1$ for fixed values of the liquid crystal material parameters and fixed surface anchoring strengths. Note that $1/l_1 \sim d^2$, and thus D is a scaled cell thickness. The case of $y_{max} = 0$ is a solution for all values of D, although not necessarily the stable solution. The case of $y_{max} \neq 0$ is a solution only for certain values of D, and when it exists it is always the stable solution. In the case of strong anchoring at both plates Palffy-Muhoray *et al.* [8] found that when the cell thickness is large, the $y_{max} \neq 0$ case is always a solution. When the anchoring is weak, we find a similar result: for $D > D_C$ bend occurs. However, as D decreases, the sequence of configurations is as follows: bend, non-bend, bend, non-bend, where the re-entrance of bend (between points A and B in figure 2) depends on the anchoring strength coefficients.

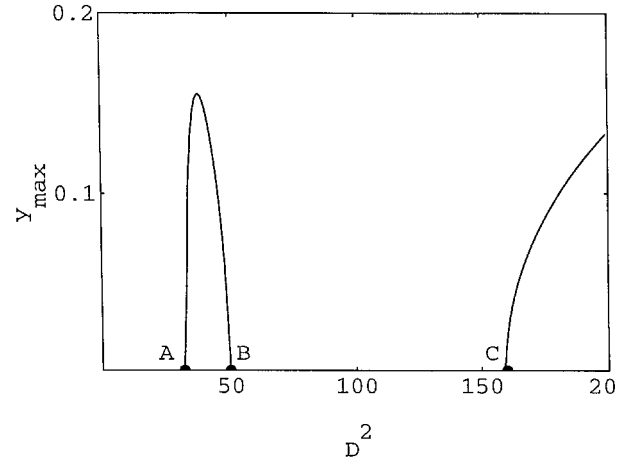

Figure 2. Order parameter y_{max} as a function of D^2 for $a = 0$, $b = 1/6^{1/2}$, $l_2 = 0$, $G_1 = 0{\cdot}05|B_1|$, $S_1 = 1{\cdot}3$, and $1/S_0 = 150$.

4.1. *Configurations*

The nematic director is associated with that eigenvector of the tensor order parameter which corresponds to the eigenvalue with the largest magnitude. The nematic is uniaxial if the other two eigenvalues are equal, and biaxial if they are not. When no bend occurs, the boundary conditions for the problem are satisfied by a configuration where the largest eigenvalue is associated with a different eigenvector in different regions of the cell. This type of configuration was named an 'eigenvalue exchange' configuration by Palffy-Muhoray *et al.* [8]. When an eigenvalue exchange occurs, the nematic director changes its orientation discontinuously. Typical cases of eigenvalue exchanges are shown in figure 3. Since in all cases $y = 0$ throughout the cell, the tensor order parameter is diagonal, and the eigenvalues are simply the diagonal elements Q_{11}, Q_{22}, and Q_{33}. In figure 3 (*a*) only one eigenvalue exchange can be seen; the exchange occurs where Q_{22} changes its sign. If we denote with $\eta = \eta_{22}$ the point where $Q_{22} = 0$, then for $\eta < \eta_{22}$ the director is ξ and the molecules on average are oriented perpendicularly to the plates. For $\eta > \eta_{22}$ the largest, in magnitude, eigenvalue is Q_{33} which is negative, showing that the orientation is in a plane perpendicular to ζ, which is called a planar alignment. Thus, the orientation

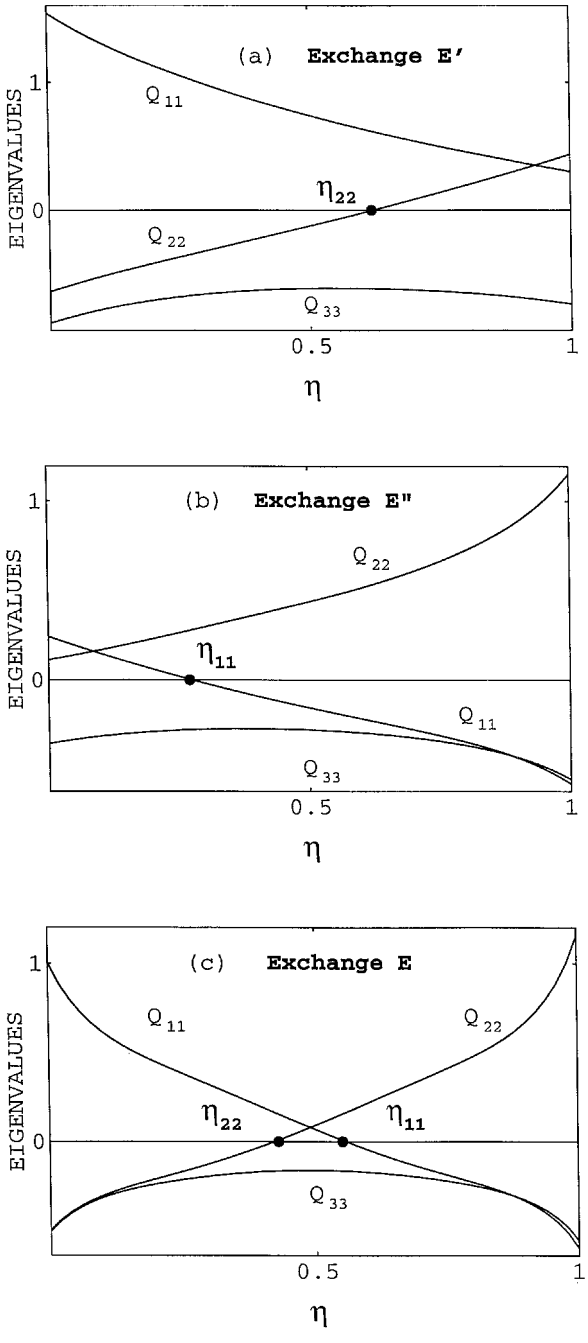

Figure 3. Eigenvalues of the tensor order parameter for the eigenvalue exchange configurations for $a=0$, $b=1/6^{1/2}$, $l_2=0$, and $G_1=0{\cdot}05|B_1|$: (*a*) one eigenvalue exchange ($\mathbf{E}'$) close to the homogeneous plate for $1/S_0=0{\cdot}5$ and $D=2$; (*b*) one eigenvalue exchange ($\mathbf{E}''$) close to the homeotropic plate for $1/S_0=10$ and $D=15$; (*c*) two eigenvalue exchanges ($\mathbf{E}$) for $1/S_0=100$ and $D=100$.

changes from homeotropic to planar at η_{22}. In figure 3 (*a*) the eigenvalue exchange occurs close to the homogeneous surface. Figure 3 (*b*) also shows one eigenvalue exchange, but now the exchange occurs close to the homeotropic plate. If η_{11} is the point where $Q_{11}=0$, then for $\eta>\eta_{11}$ the director is $\hat{v}$, and for $\eta<\eta_{11}$ it is ζ. Thus, the orientation changes from planar to parallel to the rubbed direction at η_{11}. We name the configurations shown in figure 3 (*a*) and (*b*), $\mathbf{E}'$ and $\mathbf{E}''$, respectively. Figure 3 (*c*) shows a configuration where two eigenvalue exchanges occur. For $\eta>\eta_{11}$ the molecules on average are oriented parallel to the rubbed direction $\hat{v}$. For $\eta<\eta_{22}$ the orientation is perpendicular to the plates and for $\eta_{22}<\eta<\eta_{11}$ the order is planar. We call this configuration $\mathbf{E}$.

For very small cell thickness, there are configurations where no bend or eigenvalue exchanges occur, but the bend angle θ remains either 0° or 90° depending upon the dominant surface interaction. Figure 4 shows the eigenvalues for the configurations $\theta=0$ and $\theta=\pi/2$. As can be seen, the largest eigenvalue is associated with the same eigenvector throughout the cell. The director is ξ for the $\theta=0$ and $\hat{v}$ for the $\theta=\pi/2$ configuraitons. For the $\theta=0$ configuration, the biaxiality increases when the homogeneous plate is approached. For the $\theta=\pi/2$

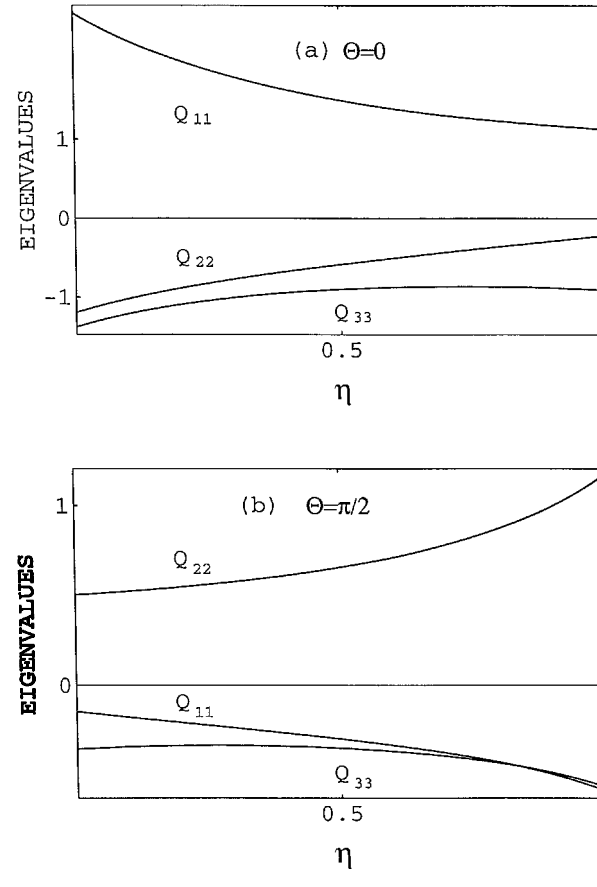

Figure 4. Eigenvalues of the tensor order parameter for the constant angle configurations for $a=0$, $b=1/6^{1,2}$, $l_2=0$, and $G_1=0{\cdot}05|B_1|$: (*a*) $\theta=0°$ for $1/S_0=0{\cdot}1$ and $D=0{\cdot}6$; (*b*) $\theta=\pi/2$ for $1/S_0=10$ and $D=5$.

configuration the opposite occurs: the nematic is more biaxial at the homeotropic plate.

In the case when the director bends continuously between the plates, y varies throughout the cell, and the tensor order parameter is not diagonal. Figure 5 shows the eigenvalues E_1, E_2, and E_3 of the tensor order parameter, and the change in the bend angle when director bend occurs. As can be seen in figure 5 (*a*), the bulk nematic exhibits considerable biaxiality; this biaxiality decreases when the cell thickness is increased. In the limit of an infinitely thick cell both the bulk and the surfaces become uniaxial, the degree of order S does not change, and the bend angle θ varies linearly with η. This is the usual behaviour known from applying Frank elastic theory to the problem of a bend cell.

4.2. *Phase diagrams*

Phase diagrams were calculated in the $1/S_0 - D^2$ plane for a set of different values of S_1, where $S_0 = G_0/(L_1 C)^{1/2}$ and $S_1 = B_1/(L_1 C)^{1/2}$ are dimensionless anchoring strength coefficients. The anchoring strength coefficient G_1 was chosen to be two orders of magnitude smaller than B_1 for any choice of B_1, thus causing a small amount of biaxiality at the homogeneous surface. The parameters A, B, C, and L_1, entering the Landau–de Gennes free energy expression [equation (8)] were held fixed in all calculations. Since S_0 is proportional to the homeotropic anchoring strength, and S_1 is proportional to the polar anchoring strength at the homogeneous plate, the phase diagrams show the possible configurations in terms of thickness and polar anchoring strengths.

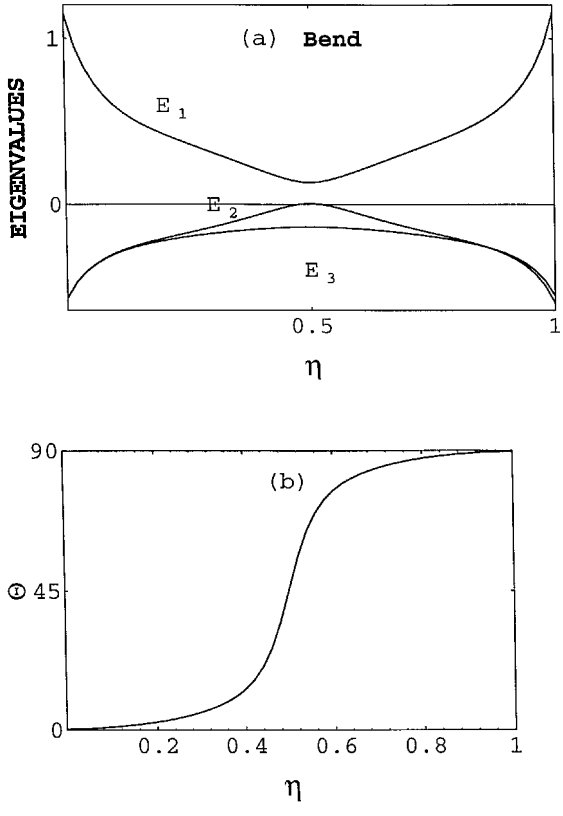

Figure 5. Bend configuration for $a = 0$, $b = 1/6^{1,2}$, $l_2 = 0$, and $G_1 = 0{\cdot}05|B_1|$; (*a*) eigenvalues of the tensor order parameter for $1/S_0 = 10$ and $D = 180$; (*b*) bend angle for $1/S_0 = 10$ and $D = 180$.

The phase diagrams obtained for a set of decreasing values of S_1 are shown in figures 6–9. Note that in all diagrams the horizontal axis is $1/S_0$ and, thus, strong anchoring corresponds to the axis origin. The configurations for $S_1 = 1{\cdot}3$ are shown in figure 6. Figure 6 (*a*) does not start at the origin and the part of the diagram that is left out is shown in figure 6 (*b*). For comparatively weak homeotropic anchoring, the bend configuration is the stable solution down to very small thickness where a continuous transition to the **E″** configuration occurs. The **E″** configuration, where one eigenvalue exchange occurs close to the homeotropic plate, is a solution in a very narrow region. When the cell thickness is decreased, the position where the eigenvalue exchange occurs [figure 3 (*b*)] moves closer and closer to the homeotropic plate until it finally 'escapes' from the cell and the $\theta = \pi/2$ configuration is obtained. The dashed line in the figure denotes the boundary between the **E″** and $\theta = \pi/2$, but no transition occurs along a dashed line. The **E″** configuration simply evolves to the $\theta = \pi/2$ configuration.

For stronger homeotropic anchoring a transition from the bend to the exchange **E** configuration occurs at larger cell thickness, and the bend configuration is re-entered at small cell thickness. When the cell thickness is decreased further, again a transition to the **E″** configuration occurs and this configuration eventually evolves to $\theta = \pi/2$. For values of S_0 such that S_0 is of the order of S_1 or a little weaker, there is no re-entrance to the bend phase at smaller cell thickness. Now with decreasing cell thickness, the positions where the two eigenvalue exchanges of the **E** configuration occur move closer and closer to the homeotropic plate until they escape from the sample one by one. Thus, the configuration **E** evolves to the **E″** configuration, and the **E″** evolves to $\theta = \pi/2$ when the cell thickness is decreased.

When the homeotropic anchoring is stronger than the polar anchoring at the homogeneous plate [figure 6 (*b*)], with decreasing cell thickness the exchange **E** configuration first evolves to the **E′** configuration with one eigenvalue exchange close to the homogeneous plate. When the cell thickness is decreased further, the **E** configuration is re-entered, after which it evolves to $\theta = \pi/2$ going through **E″**. For very strong homeotropic anchoring, when the cell thickness is decreased the **E′**

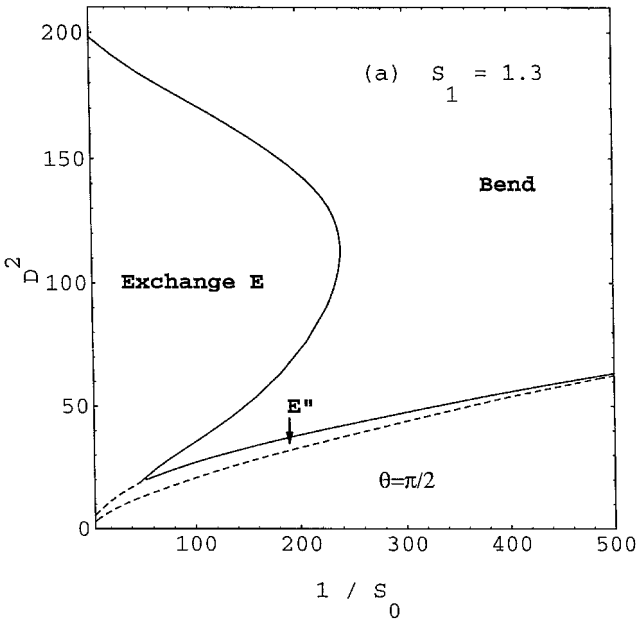

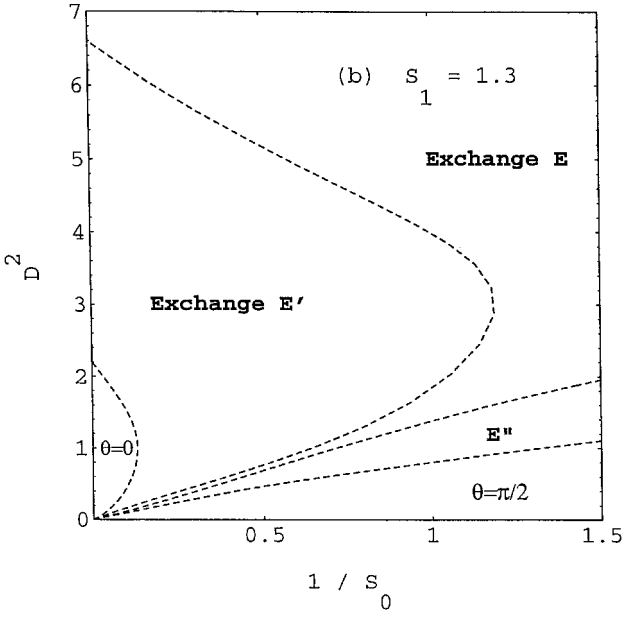

Figure 6. Phase diagram in the $1/S_0 - D^2$ plane for $a = 0$, $b = 1/6^{1/2}$, $l_2 = 0$, $G_1 = 0{\cdot}05|B_1|$, and $S_1 = 1{\cdot}3$; (*a*) weak homeotropic anchoring; (*b*) strong homeotropic anchoring.

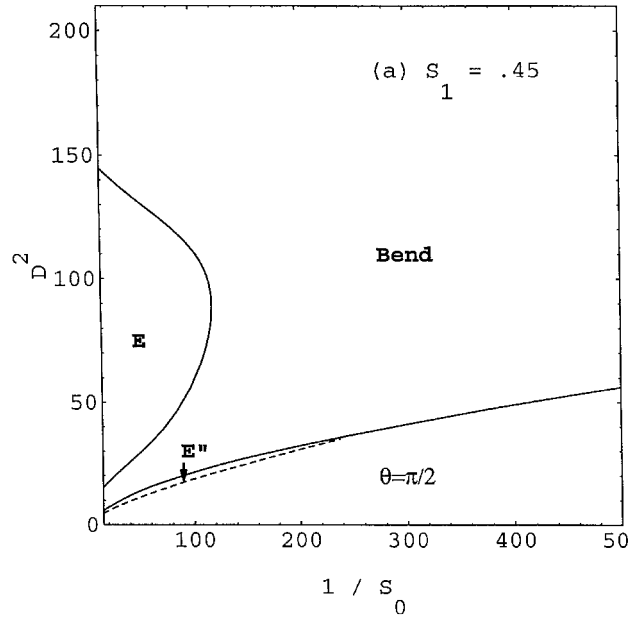

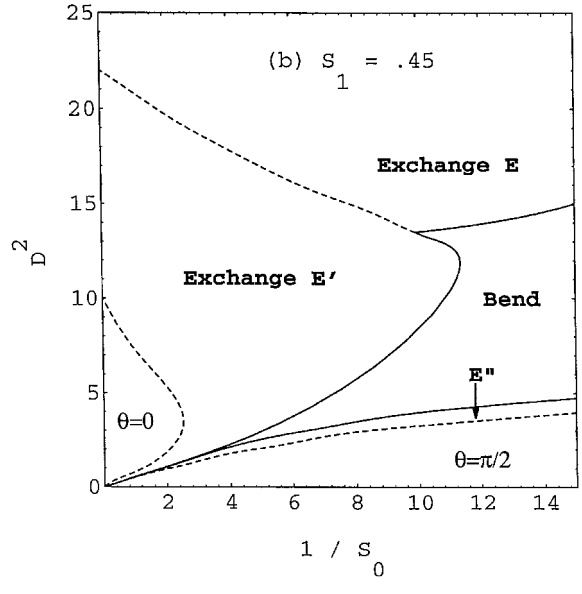

Figure 7. Phase diagram in the $1/S_0 - D^2$ plane for $a = 0$, $b = 1/6^{1/2}$, $l_2 = 0$, $G_1 = 0{\cdot}05|B_1|$, and $S_1 = 0{\cdot}45$; (*a*) weak homeotropic anchoring; (*b*) strong homeotropic anchoring.

configuration evolves to $\theta = 0$, and $\mathbf{E}'$ is re-entered at smaller cell thickness. The $\mathbf{E}'$ configuration evolves consecutively to $\mathbf{E}$, $\mathbf{E}''$, and $\theta = \pi/2$ when the cell thickness is decreased further.

The possible configurations for the case of $S_1 = 0{\cdot}45$ are shown in figure 7. It can be seen that the phase diagram has undergone several changes. The region of the $\mathbf{E}''$ configuration has become smaller and the same has happened to the exchange $\mathbf{E}$ configuration [figure 7 (*a*)]. The region where the bend configuration occurs at small cell thickness is now stable even for very strong anchoring. In figure 7 (*b*) it can be seen that the bend solution can also be re-entered from the $\mathbf{E}'$ configuration and that the regions of the $\mathbf{E}'$ and $\theta = 0$ configurations have become larger.

Figure 8 shows the possible configurations when $S_1 = 0{\cdot}27$. Here the regions of the $\mathbf{E}''$ and $\mathbf{E}$ configurations

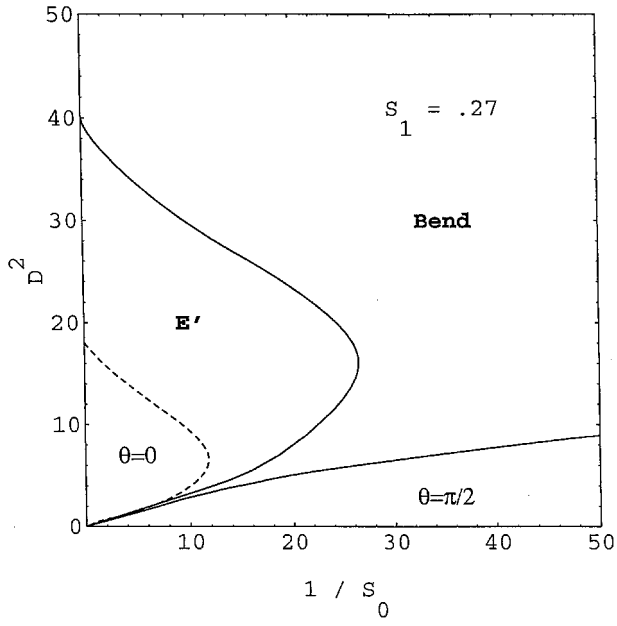

Figure 8. Phase diagram in the $1/S_0 - D^2$ plane for $a = 0$, $b = 1/6^{1/2}$, $l_2 = 0$, $G_1 = 0{\cdot}05|B_1|$, and $S_1 = 0{\cdot}27$.

have disappeared completely and the regions of the **E**′ and $\theta = 0$ have become larger. In figure 9, where $S_1 = 0{\cdot}13$, the region of the **E**′ configuration has become very small and it disappears for smaller values of S_1. When S_1 is decreased further, the only possible non-bend configurations become $\theta = 0$ and $\theta = \pi/2$, and there are no eigenvalue exchange configurations.

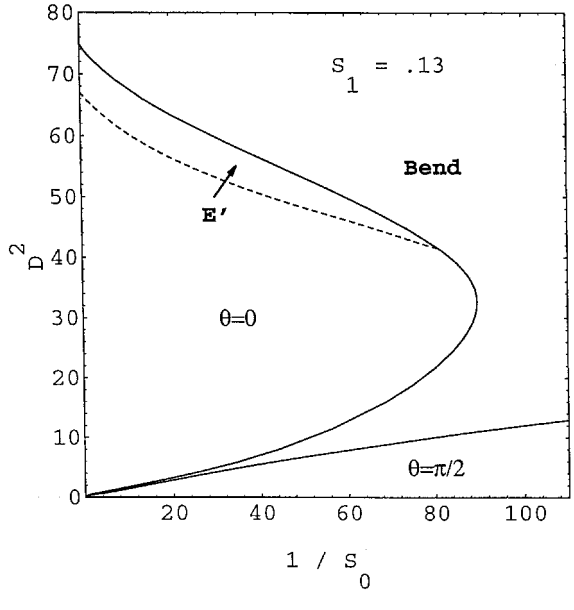

Figure 9. Phase diagram in the $1/S_0 - D^2$ plane for $a = 0$, $b = 1/6^{1/2}$, $l_2 = 0$, $G_1 = 0{\cdot}05|B_1|$, and $S_1 = 0{\cdot}13$.

5. Concluding remarks

According to the results discussed in the previous sections, the configurations that may occur in a hybrid nematic cell depend strongly on the surface anchoring strengths and cell thickness. For large cell thickness the configuration where the director bends continuously between the bounding surfaces is always stable regardless of the surface anchoring strengths. For an eigenvalue exchange configuration to occur, the cell must be sufficiently thin. Taking $A = 0$, $L_1 \sim 10^{-11}\,\mathrm{J\,m^{-1}}$ and $B \approx C = 0{\cdot}5 \times 10^6\,\mathrm{J\,m^{-3}}$ for MBBA [24], the required cell thickness is in the range of 10^{-2} to $10^{-1}\,\mu\mathrm{m}$. This estimation strongly depends on the magnitude of L_1 and on A (i.e. the temperature). The eigenvalue exchange configuration could be possible in thicker cells for liquid crystals with larger elastic constants, or at higher temperature.

When the thickness requirement is satisfied, which configuration is stable depends upon the anchoring strengths. Taking into account how the regions of the various configurations change for different values of S_1, it can be concluded that configurations of the eigenvalue exchange type may occur for comparatively strong S_1 and S_0 of the same order or stronger.

All results were obtained using the equal elastic constants approximation ($l_2 = 0$), keeping the temperature at the supercooling limit ($a = 0$), and setting $B/C = 1$. Calculations performed with $l_2 \neq 0$ did not show any considerable effect on the phase diagrams. The results, however, are very sensitive to temperature and the B/C ratio. For $a > 0$ and $B/C < 1$ the region **E** where two eigenvalue exchanges occur expands very rapidly to larger D. If the nematic to isotropic transition does not occur first, the eigenvalue exchange configuration may be observable even for conventional liquid crystals in a narrow temperature interval in cells about 1 μm thick. Thus, eigenvalue exchange configurations may be found in cells with liquid crystals having small B and large elastic constants at temperatures close to the clearing point.

Another way to look for configurations of the eigenvalue exchange type is in liquid crystals confined to materials, e.g. Silica Aerogel or Vycor glass, which have very small pore sizes: 0·0175 and 0·007 μm, respectively [25]. However, a difficulty with these materials is that the pore shapes and anchoring strengths cannot be reliably controlled.

This work was supported by the National Science Foundation under the Science and Technology Center ALCOM Grant No. DMR89-20147.

References

[1] Frank, F. C., 1958, *Discuss. Faraday Soc.*, **25,** 19.
[2] Ericksen, J. L., 1991, *Arch. Ration. Mech. Anal.*, **113,** 97.

[3] MIZEL, V. J., ROCCATO, D., and VIRGA, E. G., 1991, *Arch. Ration. Mech. Anal.*, **116,** 115.
[4] AMBROSIO, L., and VIRGA, E. G., 1991, *Arch. Ration. Mech. Anal.*, **114,** 335.
[5] ROCCATO, D., and VIRGA, E. G., 1992, *Continuum Mech. Thermodyn.*, **4,** 121.
[6] DE GENNES, P. G., and PROST, J., 1993, *The Physics of Liquid Crystals* (Oxford: Clarendon Press).
[7] GARTLAND, E. C., JR, MUHORAY-PALFFY, P., and VARGA, R. S., 1991, *Mol. Cryst. liq. Cryst.*, **199,** 429.
[8] PALFFY-MUHORAY, P., GARTLAND, E. C., and KELLY, J. R., 1994, *Liq. Cryst.*, **1,** 713.
[9] KOTHEKAR, N., and ALLENDER, D. W. (in press).
[10] SHENG, P., 1976, *Phys. Rev. Lett.*, **37,** 1059.
[11] ALLENDER, D. W., HENDERSON, G. L., and JOHNSON, D. L., 1981, *Phys. Rev. A*, **24,** 1086.
[12] SHENG, P., 1982, *Phys. Rev. A*, **26,** 1601.
[13] HORNREICH, R. M., KATS, E. I., and LEBEDEV, V. V., 1992, *Phys. Rev. A*, **46,** 4935.
[14] L'VOV, Y., HORNREICH, R. M., and ALLENDER, D. W., 1993, *Phys. Rev. E*, **48,** 1115.
[15] KOTHEKAR, N., ALLENDER, D. W., and HORNREICH, R. M., 1994, *Phys. Rev. E*, **49,** 2150.
[16] KOTHEKAR, N., ALLENDER, D. W., and HORNREICH, R. M., 1995, *Phys. Rev. E*, **52,** 4541.
[17] LAVRENTOVICH, O. D., and PERGAMENSHCHIK, V. M., 1990, *Mol. Cryst. liq. Cryst.*, **179,** 125.
[18] LAVRENTOVICH, O. D., and PERGAMENSHCHIK, V. M., 1994, *Phys. Rev. Lett.*, **73,** 979.
[19] SPARAVIGNA, A., KOMITOV, L., STEBLER, B., and STRIGAZZI, A., 1991, *Mol. Cryst. liq. Cryst.*, **207,** 265.
[20] SPARAVIGNA, A., and STRIGAZZI, A., 1992, *Mol. Cryst. liq. Cryst.*, **221,** 109.
[21] CHANDRASEKHAR, S., 1992, *Liquid Crystals* (Cambridge: Cambridge University Press).
[22] HANS SAGAN, 1961, *Boundary and Eigenvalue Problems in Mathematical Physics* (New York: John Wiley).
[23] ASCHER, U., CHRISTIANSEN, J., and RUSSEL, R. D., 1981, *ACM Trans. Math. Software*, **7,** 209.
[24] PRIESTLY, E. B., WOJTOWICZ, P. J., and SHENG, P (eds), *Introduction to Liquid Crystals* (New York and London: Plenum Press).
[25] CRAWFORD, G. P., and DOANE, J. W., 1993, *Mod. Phys. Lett. B*, **7,** 1785.